

The effect of annealing on the elastoplastic and viscoelastic responses of isotactic polypropylene

Aleksey D. Drozdov and Jesper deClaville Christiansen
Department of Production
Aalborg University
Fibigerstraede 16
DK-9220 Aalborg, Denmark

Abstract

Observations are reported on isotactic polypropylene (i) in a series of tensile tests with a constant strain rate on specimens annealed for 24 h at various temperatures in the range from 110 to 150 °C and (ii) in two series of creep tests in the sub-yield region of deformation on samples not subjected to thermal treatment and on specimens annealed at 140 °C. A model is developed for the elastoplastic and nonlinear viscoelastic responses of semicrystalline polymers. A polymer is treated as an equivalent transient network of macromolecules bridged by junctions (physical cross-links, entanglements and lamellar blocks). The network is assumed to be highly heterogeneous, and it is thought of as an ensemble of meso-regions with different activation energies for separation of strands from temporary nodes. The elastoplastic behavior is modelled as sliding of meso-domains with respect to each other driven by mechanical factors. The viscoelastic response is attributed to detachment of active strands from temporary junctions and attachment of dangling chains to the network. Constitutive equations for isothermal uniaxial deformation are derived by using the laws of thermodynamics. Adjustable parameters in the stress-strain relations are found by fitting the experimental data.

1 Introduction

This paper is concerned with the effect of annealing on the elastoplastic and viscoelastic responses of injection-molded isotactic polypropylene (iPP). This semi-crystalline polypropylene is chosen for the analysis because of its numerous applications in industry (oriented films for packaging, reinforcing fibres, nonwoven fabrics, blends with thermoplastic elastomers, etc.).

The effect of annealing at elevated temperatures on the morphology of polypropylene has been a focus of attention in past five years, see, e.g., [1, 2, 3, 4, 5, 6, 7], to mention a few. The previous works concentrated on calorimetric studies of morphological transformations driven by primary and secondary crystallization. The influence of changes in the microstructure of spherulites on the mechanical behavior of iPP was not studied in detail.

The nonlinear viscoelastic response of polypropylene was analyzed by Ward and Wolfe [8] and Smart and Williams [9] several decades ago and, in the past decade, by Wortmann and Schulz [10, 11], Ariyama [12], Ariyama et al. [13], Dutta and Edward [14], Read and Tomlins [15], Tomlins and Read [16] and Sweeney et al. [17].

Yielding and viscoplasticity of iPP have been recently investigated by Aboulfaraj et al. [18], Kalay and Bevis [1], Coulon et al. [19], Seguela et al. [20], Staniek et al. [21], Nitta and Takayanagi [22, 23] and Labour et al. [24], to mention a few.

Isotactic polypropylene is a semi-crystalline polymer containing monoclinic α crystallites, hexagonal β structures, orthorhombic γ polymorphs and “smectic” mesophase [5]. At rapid cooling of the melt (at the stage of injection molding), α crystallites and smectic mesophase are mainly developed, whereas β and γ polymorphs are observed as minority components [1, 2].

A unique feature of α spherulites in iPP is the lamellar cross-hatching: development of transverse lamellae oriented in the direction perpendicular to the direction of radial lamellae [5, 6]. The characteristic size of α spherulites in injection-molded specimens is estimated as 100 to 200 μm [1, 19]. These spherulites consist of crystalline lamellae with thickness of 10 to 20 nm [6, 19].

The amorphous phase is located (i) between spherulites, (ii) inside spherulites, in “liquid pockets” between lamellar stacks [25], and (iii) between lamellae in lamellar stacks. It consists of (i) relatively mobile chains between spherulites, in liquid pockets and between radial lamellae inside lamellar stacks, and (ii) severely restricted chains in the regions bounded by radial and tangential lamellae (rigid amorphous fraction [25]).

Stretching of iPP specimens results in inter-lamellar separation, rotation and twist of lamellae, fine and coarse slip of lamellar blocks and their fragmentation [18, 20], chain slip through the crystals, sliding, pull-out and breakage of tie chains [22, 23], and activation of rigid amorphous fraction. At large strains, these morphological transformations lead to cavitation, formation of fibrills and stress-induced crystallization of iPP [26].

To develop stress–strain relations, we apply a method of “homogenization of microstructure,” according to which a sophisticated morphology of isotactic polypropylene is modelled by an equivalent phase whose deformation captures essential features of the mechanical response. An amorphous phase is chosen as the equivalent phase for the following reasons:

1. The viscoelastic response of isotactic polypropylene is conventionally associated with rearrangement of chains in amorphous regions [19].
2. Sliding of tie chains along and their detachment from lamellae play the key role in the time-dependent response of iPP [22, 23].
3. The viscoplastic flow in semi-crystalline polymers is assumed to be “initiated in the amorphous phase before transitioning into the crystalline phase” [27].
4. The time-dependent behavior of polypropylene is conventionally modelled within the concept of a network of macromolecules [17, 28].

Dynamic mechanical analysis reveals that the loss tangent of iPP demonstrates two pronounced maxima being plotted versus temperature [20, 29]. The first maximum (β -transition in the interval between $T = -20$ and $T = 10$ °C) is associated with the glass

transition in a mobile part of the amorphous phase, whereas the other maximum (α -transition in the interval between $T = 70$ and $T = 110$ °C) is attributed to the glass transition in the remaining part of the amorphous phase, the rigid amorphous fraction [25].

At room temperature (i.e., above the glass transition temperature for the mobile amorphous phase) iPP is treated a transient network of macromolecules [30] bridged by junctions (physical cross-links, entanglements and lamellar blocks). The network is assumed to be highly heterogeneous (the inhomogeneity is attributed to interactions between spherulites and amorphous regions, as well as to local density fluctuations in the amorphous phase), and it is thought of as an ensemble of meso-regions (MRs) with different activation energies for separation of strands from temporary nodes.

Two types of MRs are distinguished: (i) active domains, where strands separate from junctions as they are thermally agitated (mobile part of the amorphous phase), and (ii) passive domains, where detachment of chains from junctions is prevented by surrounding lamellae.

Stretching of a specimen induces

1. slippage of meso-domains with respect to each other (which models the elastoplastic behavior of iPP),
2. separation of active strands from temporary junctions and attachment of dangling chains to the network in active meso-regions (which reflects the viscoelastic response),
3. an increase in the content of active MRs driven by release of the rigid amorphous fraction due to lamellar fragmentation (which is associated with the nonlinearity of the viscoelastic behavior in the sub-yield region of deformation).

The objective of this study is three-fold:

1. To report experimental data in tensile tests with a constant strain rate on specimens annealed at various temperatures in the interval between 110 and 150 °C.
2. To present observations in creep tests on non-annealed samples and on specimens annealed at 140 °C in the sub-yield region.
3. To derive constitutive equations for the time-dependent behavior of a semicrystalline polymer and to find adjustable parameters in the stress–strain relations by fitting observations.

The goal of this paper is to shed some light on correlations between morphological transformations in iPP at annealing and changes in stress–strain diagrams and creep curves measured in the sub-yield and post-yield regions of deformation.

The exposition is organized as follows. The specimens and the experimental procedure are described in Section 2. Section 3 deals with kinetic equations for rearrangement of strands in active meso-domains. Sliding of MRs with respect to each other is described in Section 4. Stress–strain relations are derived in Section 5 by using the laws of thermodynamics. Adjustable parameters in the constitutive equations are found in Section 6

by fitting observations. A brief discussion of our findings is presented in Section 7. Some concluding remarks are formulated in Section 8.

2 Experimental procedure

Isotactic polypropylene (Novolen 1100L) was supplied by BASF (Targor). ASTM dumb-bell specimens were injection molded with length 148 mm, width 10 mm and height 3.8 mm. Mechanical tests were performed on non-annealed specimens, as well as on samples annealed in an oven for 24 h at the temperatures 110, 120, 130, 140 and 150 °C. After annealing, the specimens were slowly cooled by air. To minimize the effect of physical aging on the time-dependent response, tests were carried out a week after thermal pre-treatment.

Uniaxial tensile tests were performed at room temperature on a testing machine Instron-5568 equipped with electro-mechanical sensors for the control of longitudinal strains in the active zone of samples (with the distance 50 mm between clips). The tensile force was measured by a standard load cell. The longitudinal stress, σ , was determined as the ratio of the axial force to the cross-sectional area of stress-free specimens.

In the first series of tests, non-annealed specimens and specimens annealed at various temperatures, T , were loaded with the cross-head speed 5 mm/min (that corresponded to the Hencky strain rate $\dot{\epsilon}_H = 1.1 \cdot 10^{-3} \text{ s}^{-1}$) up to the maximal strain $\epsilon_{\max} = 0.06$. According to [31], the chosen strain rate ensured nearly isothermal test conditions. The engineering stress, σ , was plotted versus the longitudinal strain, ϵ , in Figure 1.

A series of 6 creep tests was performed on non-annealed specimens at the longitudinal stresses $\sigma_1^0 = 10.0 \text{ MPa}$, $\sigma_2^0 = 15.0 \text{ MPa}$, $\sigma_3^0 = 17.5 \text{ MPa}$, $\sigma_4^0 = 20.0 \text{ MPa}$, $\sigma_5^0 = 22.5 \text{ MPa}$ and $\sigma_6^0 = 25.0 \text{ MPa}$. Each creep test was carried out on a new sample. In the m th test ($m = 1, \dots, 6$), a specimen was loaded with the cross-head speed 5 mm/min up to the engineering stress σ_m^0 that was preserved constant during the creep test, $t_c = 20 \text{ min}$. The longitudinal strain, ϵ , was plotted versus the logarithm ($\log = \log_{10}$) of time t (the instant $t = 0$ corresponds to the beginning of a creep test) in Figure 2.

To evaluate the effect of annealing on the nonlinear viscoelastic behavior of iPP, a series of 5 creep tests was performed on specimens annealed at 140 °C at the longitudinal stresses $\sigma_1^0 = 10.0 \text{ MPa}$, $\sigma_2^0 = 15.0 \text{ MPa}$, $\sigma_3^0 = 20.0 \text{ MPa}$, $\sigma_4^0 = 25.0 \text{ MPa}$, and $\sigma_5^0 = 30.0 \text{ MPa}$. The strain, ϵ , was plotted versus the logarithm of time, t , in Figure 3.

Figures 2 and 3 demonstrate that the rate of increase in strain, ϵ , with time, t , is relatively low at small stresses, and it noticeably grows with the longitudinal stress, σ . Our aim is to derive constitutive equations for the elastoplastic and viscoelastic responses of a semi-crystalline polymer and to find adjustable parameters in the stress-strain relations by fitting the experimental data plotted in Figures 1 to 3.

3 Rearrangement of strands in active meso-regions

A semicrystalline polymer is treated as a transient network of macromolecules bridged by temporary nodes. The network is modelled as an ensemble of meso-regions with various

potential energies for detachment of strands from their junctions. Two types of meso-domains are distinguished:

1. passive, where all nodes are thought of as permanent,
2. active, where active strands (whose ends are connected to contiguous junctions) separate from the nodes at random times when these strands are thermally agitated.

An active chain whose end detaches from a junction is transformed into a dangling chain. A dangling chain returns into the active state when its free end captures a nearby junction at a random instant.

Denote by X_a the number (per unit mass) of active strands in active MRs, and by X_p the number (per unit mass) of strands connected to the network in passive MRs. Under a time-dependent loading program, some lamellae (restricting mobility of chains in passive MRs) break, which results in an increase in the number of strands to be rearranged. The quantities X_a and X_p are treated as functions of time, t , that obey the conservation law

$$X_a(t) + X_p(t) = X, \quad (1)$$

where X is the average number of active strands per unit mass of a polymer (which is assumed to be time-independent).

Rearrangement of strands in active MRs is thought of as a thermally activated process. The rate of detachment of active strands from their junctions in a MR with potential energy $\bar{\omega}$ is given by the Eyring equation [32]

$$\Gamma = \Gamma_a \exp\left(-\frac{\bar{\omega}}{k_B T}\right),$$

where k_B is Boltzmann's constant, T is the absolute temperature, and the pre-factor Γ_a is independent of energy $\bar{\omega}$ and temperature T . Confining ourselves to isothermal deformations at a reference temperature T_0 and introducing the dimensionless activation energy $\omega = \bar{\omega}/(k_B T_0)$, we arrive at the formula

$$\Gamma = \Gamma_a \exp(-\omega). \quad (2)$$

An ensemble of active MRs with various potential energies is described by the distribution function $p(t, \omega)$ that equals the ratio of the number, $N_a(t, \omega)$, of active meso-domains with energy ω at instant t to the total number of active MRs,

$$p(t, \omega) = \frac{N_a(t, \omega)}{X_a(t)}, \quad X_a(t) = \int_0^\infty N_a(t, \omega) d\omega, \quad (3)$$

and by the concentration of active MRs

$$\kappa_a(t) = \frac{X_a(t)}{X}. \quad (4)$$

In what follows, constitutive equations will be derived for an arbitrary distribution function $p(t, \omega)$. To fit experimental data, a random energy model is applied with

$$p(t, \omega) = p_0(t) \exp\left[-\frac{(\omega - \Omega(t))^2}{2\Sigma^2(t)}\right] \quad (\omega \geq 0), \quad p(t, \omega) = 0 \quad (\omega < 0), \quad (5)$$

where Ω is the average activation energy in an ensemble of active meso-domains, Σ is the standard deviation of potential energies for separation of strands, and $p_0(t)$ is determined by the condition

$$\int_0^\infty p(t, \omega) d\omega = 1. \quad (6)$$

An ensemble of active meso-domains is characterized by the function $n_a(t, \tau, \omega)$ that equals the number (per unit mass) of active strands at time t belonging to active MRs with potential energy ω that have last been rearranged before instant $\tau \in [0, t]$. In particular, $n_a(t, t, \omega)$ is the number (per unit mass) of active strands in active MRs with potential energy ω at time $t \geq 0$,

$$n_a(t, t, \omega) = N_a(t, \omega). \quad (7)$$

The amount $\varphi(\tau, \omega) d\tau$, where

$$\varphi(\tau, \omega) = \left. \frac{\partial n_a}{\partial \tau}(t, \tau, \omega) \right|_{t=\tau}, \quad (8)$$

equals the number (per unit mass) of dangling strands in active MRs with potential energy ω that merge with the network within the interval $[\tau, \tau + d\tau]$, and the quantity

$$\frac{\partial n_a}{\partial \tau}(t, \tau, \omega) d\tau$$

is the number of these strands that have not detached from temporary junctions during the interval $[\tau, t]$. The number (per unit mass) of strands in active MRs that separate (for the first time) from the network within the interval $[t, t + dt]$ reads

$$-\frac{\partial n_a}{\partial t}(t, 0, \omega) dt.$$

The number (per unit mass) of strands in active MRs that merged with the network during the interval $[\tau, \tau + d\tau]$ and, afterwards, separated from the network within the interval $[t, t + dt]$ is given by

$$-\frac{\partial^2 n_a}{\partial t \partial \tau}(t, \tau, \omega) dt d\tau.$$

The rate of detachment, Γ , equals the ratio of the number of active strands that separate from the network per unit time to the current number of active strands. Applying this definition to active strands that merged with the network during the interval $[\tau, \tau + d\tau]$ and separated from temporary junctions within the interval $[t, t + dt]$, we find that

$$\frac{\partial^2 n_a}{\partial t \partial \tau}(t, \tau, \omega) = -\Gamma(\omega) \frac{\partial n_a}{\partial \tau}(t, \tau, \omega). \quad (9)$$

Changes in the function $n_a(t, 0, \omega)$ are governed by two processes:

1. detachment of active strands from temporary nodes,
2. mechanically-induced activation of passive MRs.

The kinetic equation for this function reads

$$\frac{\partial n_a}{\partial t}(t, 0, \omega) = -\Gamma(\omega)n_a(t, 0, \omega) + \frac{\partial N_a}{\partial t}(t, \omega). \quad (10)$$

The solution of Eq. (10) with initial condition (7), where we set $t = 0$, is given by

$$n_a(t, 0, \omega) = N_a(0, \omega) \exp[-\Gamma(\omega)t] + \int_0^t \frac{\partial N_a}{\partial t}(\tau, \omega) \exp[-\Gamma(\omega)(t - \tau)] d\tau. \quad (11)$$

It follows from Eqs. (8) and (9) that

$$\frac{\partial n_a}{\partial \tau}(t, \tau, \omega) = \varphi(\tau, \omega) \exp[-\Gamma(\omega)(t - \tau)]. \quad (12)$$

Equation (7) implies that

$$N_a(t, \omega) = n_a(t, 0, \omega) + \int_0^t \frac{\partial n_a}{\partial \tau}(t, \tau, \omega) d\tau. \quad (13)$$

Differentiating Eq. (13) with respect to time and using Eq. (8), we find that

$$\varphi(t, \omega) + \frac{\partial n_a}{\partial t}(t, 0, \omega) + \int_0^t \frac{\partial^2 n_a}{\partial t \partial \tau}(t, \tau, \omega) d\tau = \frac{\partial N_a}{\partial t}(t, \omega).$$

This equality together with Eqs. (9), (10) and (13) results in

$$\varphi(t, \omega) = \Gamma(\omega)N_a(t, \omega).$$

This expression together with Eq. (12) yields

$$\frac{\partial n_a}{\partial \tau}(t, \tau, \omega) = \Gamma(\omega)N_a(t, \omega) \exp[-\Gamma(\omega)(t - \tau)]. \quad (14)$$

Rearrangement of strands in active MRs is described by Eqs. (2), (11) and (14). Separation of active strands from their junctions and detachment of dangling chains to the network reflect the viscoelastic response of a semi-crystalline polymer.

4 Sliding of meso-regions

It is assumed that meso-domains are not rigidly connected, but can slide with respect to each other under straining. Sliding of meso-domains is treated as a rate-independent process and is associated with the elastoplastic behavior of a semi-crystalline polymer. We suppose that an increase in strain, ϵ , by an increment, $d\epsilon$, causes growth of the elastoplastic strain, ϵ_p , by an increment, $d\epsilon_p$, that is proportional to $d\epsilon$,

$$d\epsilon_p = \Psi d\epsilon.$$

The coefficient of proportionality, Ψ , depends, in general, on the macro-strain, ϵ , the macro-stress, σ , and the elastoplastic strain, ϵ_p . We presume that Ψ is a function of the

elastic strain, ϵ_e , which is defined as the difference between the macro-strain, ϵ , and the elastoplastic strain, ϵ_p ,

$$\epsilon_e(t) = \epsilon(t) - \epsilon_p(t). \quad (15)$$

This results in the kinetic equation

$$\frac{d\epsilon_p}{dt}(t) = \Psi(\epsilon(t) - \epsilon_p(t)) \frac{d\epsilon}{dt}(t), \quad \epsilon_p(0) = 0. \quad (16)$$

It is natural to suppose that the function $\Psi(\epsilon_e)$ vanishes at $\epsilon_e = 0$ (no elastoplastic strains are observed at small macro-strains), monotonically increases with the elastic strain, and reaches some limiting value $b \in (0, 1)$ at large values of ϵ_e (which corresponds to a steady regime of plastic flow). To minimize the number of adjustable parameters in constitutive equations, an exponential dependence is adopted,

$$\Phi(\epsilon_e) = b[1 - \exp(-a\epsilon_e)], \quad (17)$$

where the positive coefficients a and b are found by matching observations. It is worth noting that Eqs. (16) and (17) differ from conventional flow rules in elastoplasticity, where the elastoplastic strain is assumed to be proportional to stress, σ . These equations are, however, in good agreement with the conclusion by Men and Strobl [33] that “tensile deformations of semi-crystalline polymers . . . are strain-controlled.”

5 Constitutive equations

An active strand is modelled as a linear elastic medium with the mechanical energy

$$w(t) = \frac{1}{2}\mu e^2(t), \quad (18)$$

where μ is the average rigidity per strand and e is the strain from the stress-free state to the deformed state of the strand.

For strands belonging to passive meso-domains, the strain e coincides with the elastic strain ϵ_e . Multiplying the strain energy per strand, Eq. (18), by the number of strands in passive MRs, we find the mechanical energy of meso-domains where rearrangement of chains is prevented by surrounding lamellae,

$$W_p(t) = \frac{1}{2}\mu X_p(t)\epsilon_e^2(t). \quad (19)$$

With reference to the conventional theory of temporary networks [30], stresses in dangling strands are assumed to totally relax before these strands merge with the network. This implies that the reference (stress-free) state of a strand that is attached to the network at time τ coincides with the deformed state of the network at that instant. For active strands that have not been rearranged until time t , the strain $e(t)$ coincides with $\epsilon_e(t)$, whereas for active strands that have last been merged with the network at time $\tau \in [0, t]$, the strain $e(t, \tau)$ is given by

$$e(t, \tau) = \epsilon_e(t) - \epsilon_e(\tau).$$

Summing the mechanical energies of active strands belonging to active MRs with various potential energies, ω , that were rearranged at various instants, $\tau \in [0, t]$, we find the strain energy of active meso-domains,

$$W_a(t) = \frac{1}{2}\mu \int_0^\infty \left\{ n_a(t, 0, \omega) \epsilon_e^2(t) + \int_0^t \frac{\partial n_a}{\partial \tau}(t, \tau, \omega) [\epsilon_e(t) - \epsilon_e(\tau)]^2 d\tau \right\} d\omega. \quad (20)$$

The mechanical energy per unit mass of a polymer reads

$$W(t) = W_a(t) + W_p(t).$$

It follows from this equality and Eqs. (15), (19) and (20) that

$$\begin{aligned} W(t) = & \frac{1}{2}\mu \left\{ X_p(t) (\epsilon(t) - \epsilon_p(t))^2 + \int_0^\infty \left[n_a(t, 0, \omega) (\epsilon(t) - \epsilon_p(t))^2 \right. \right. \\ & \left. \left. + \int_0^t \frac{\partial n_a}{\partial \tau}(t, \tau, \omega) \left((\epsilon(t) - \epsilon_p(t)) - (\epsilon(\tau) - \epsilon_p(\tau)) \right)^2 d\tau \right] d\omega \right\}. \end{aligned} \quad (21)$$

Our aim now is to calculate the derivative of the function $W(t)$ with respect to time t . Differentiation of Eq. (21) results in

$$\frac{dW}{dt}(t) = A(t) \left[\frac{d\epsilon}{dt}(t) - \frac{d\epsilon_p}{dt}(t) \right] - A_1(t), \quad (22)$$

where

$$\begin{aligned} A(t) = & \mu \left\{ X_p(t) (\epsilon(t) - \epsilon_p(t)) + \int_0^\infty \left[n_a(t, 0, \omega) (\epsilon(t) - \epsilon_p(t)) \right. \right. \\ & \left. \left. + \int_0^t \frac{\partial n_a}{\partial \tau}(t, \tau, \omega) \left((\epsilon(t) - \epsilon_p(t)) - (\epsilon(\tau) - \epsilon_p(\tau)) \right) d\tau \right] d\omega \right\}, \end{aligned} \quad (23)$$

$$\begin{aligned} A_1(t) = & -\frac{1}{2}\mu \left\{ \frac{dX_p}{dt}(t) (\epsilon(t) - \epsilon_p(t))^2 + \int_0^\infty \left[\frac{\partial n_a}{\partial t}(t, 0, \omega) (\epsilon(t) - \epsilon_p(t))^2 \right. \right. \\ & \left. \left. + \int_0^t \frac{\partial^2 n_a}{\partial t \partial \tau}(t, \tau, \omega) \left((\epsilon(t) - \epsilon_p(t)) - (\epsilon(\tau) - \epsilon_p(\tau)) \right)^2 d\tau \right] d\omega \right\}. \end{aligned} \quad (24)$$

It follows from Eqs. (1), (3), (13) and (23) that

$$A(t) = \mu \left[X (\epsilon(t) - \epsilon_p(t)) - \int_0^\infty d\omega \int_0^t \frac{\partial n_a}{\partial \tau}(t, \tau, \omega) (\epsilon(\tau) - \epsilon_p(\tau)) d\tau \right]. \quad (25)$$

Substituting Eqs. (9) and (10) into Eq. (24) and using Eqs. (1) and (3), we obtain

$$\begin{aligned} A_1(t) = & \frac{1}{2}\mu \int_0^\infty \Gamma(\omega) d\omega \left[n_a(t, 0, \omega) (\epsilon(t) - \epsilon_p(t))^2 \right. \\ & \left. + \int_0^t \frac{\partial n_a}{\partial \tau}(t, \tau, \omega) \left((\epsilon(t) - \epsilon_p(t)) - (\epsilon(\tau) - \epsilon_p(\tau)) \right)^2 d\tau \right]. \end{aligned} \quad (26)$$

For isothermal uniaxial deformation, the Clausius-Duhem inequality reads

$$Q(t) = -\frac{dW}{dt}(t) + \frac{1}{\rho} \sigma(t) \frac{d\epsilon}{dt}(t) \geq 0,$$

where ρ is mass density, and Q is internal dissipation per unit mass. Substitution of Eqs. (16) and (22) into this equation results in

$$\left[\sigma(t) - \rho A(t) \left(1 - \Psi(\epsilon(t) - \epsilon_p(t)) \right) \right] \frac{d\epsilon}{dt}(t) + \rho A_1(t) \geq 0. \quad (27)$$

It follows from Eq. (26) that the function $A_1(t)$ is non-negative for an arbitrary program of loading. This means that the dissipation inequality (27) is satisfied, provided that the expression in the square brackets vanishes. This condition together with Eq. (25) results in the stress-strain relation

$$\begin{aligned} \sigma(t) = & E \left[1 - \Psi(\epsilon(t) - \epsilon_p(t)) \right] \left[(\epsilon(t) - \epsilon_p(t)) \right. \\ & \left. - \frac{1}{X} \int_0^\infty d\omega \int_0^t \frac{\partial n_a}{\partial \tau}(t, \tau, \omega) (\epsilon(\tau) - \epsilon_p(\tau)) d\tau \right], \end{aligned}$$

where $E = \rho\mu X$ is an analog of Young's modulus. Substitution of Eqs. (3), (4) and (14) into this equality implies that

$$\begin{aligned} \sigma(t) = & E \left[1 - \Psi(\epsilon(t) - \epsilon_p(t)) \right] \left[(\epsilon(t) - \epsilon_p(t)) - \kappa_a(t) \int_0^\infty \Gamma(\omega) d\omega \right. \\ & \left. \times \int_0^t \exp(-\Gamma(\omega)(t - \tau)) (\epsilon(\tau) - \epsilon_p(\tau)) p(\tau, \omega) d\tau \right]. \end{aligned} \quad (28)$$

Given functions $p(t, \omega)$ and $\kappa_a(t)$, Eqs. (2), (16), (17) and (28) determine the time-dependent behavior of a semicrystalline polymer at isothermal uniaxial deformation.

To approximate the experimental data reported in Section 2, we concentrate on tensile tests with constant strain rates and on creep tests.

Confining ourselves to "rapid" tensile tests, when the effect of the material's viscosity on the mechanical response may be disregarded, we neglect the integral term in Eq. (28) and arrive at the constitutive equation

$$\sigma(t) = E \left[1 - \Psi(\epsilon(t) - \epsilon_p(t)) \right] (\epsilon(t) - \epsilon_p(t)). \quad (29)$$

Equations (16), (17) and (29) are determined by 3 material parameters:

1. the elastic modulus E ,
2. the constant a that characterizes the rate of elastoplastic strain,
3. the constant b that describes a developed plastic flow.

It is natural to assume that in a standard creep test with a longitudinal stress σ^0 ,

$$\sigma(t) = \begin{cases} 0, & t < 0, \\ \sigma^0, & t \geq 0, \end{cases}$$

the quantities κ_a and p are functions of the stress intensity σ^0 . It follows from Eqs. (15) and (28) that the elastic strain, ϵ_e , reads

$$\epsilon_e(t) = \frac{\sigma^0}{1 - \Psi(\epsilon_e(t))} + \kappa_a(\sigma^0) \int_0^\infty Z(t, \omega) p(\sigma^0, \omega) d\omega, \quad (30)$$

where

$$Z(t, \omega) = \Gamma(\omega) \int_0^t \exp[-\Gamma(\omega)(t - \tau)] \epsilon_e(\tau) d\tau. \quad (31)$$

Equation (31) implies that the function $Z(t, \omega)$ satisfies the differential equation

$$\frac{\partial Z}{\partial t}(t, \omega) = \Gamma(\omega) [\epsilon_e(t) - Z(t, \omega)], \quad Z(0, \omega) = 0. \quad (32)$$

After solving Eqs. (30) and (32), the longitudinal strain, ϵ , is found from Eqs. (15) and (16) which can be presented in the form

$$\frac{d\epsilon}{dt}(t) = [1 - \Psi(\epsilon_e(t))]^{-1} \frac{d\epsilon_e}{dt}(t), \quad \epsilon(0) = \epsilon^0(\sigma^0), \quad \epsilon_e(0) = \epsilon_e^0(\sigma^0), \quad (33)$$

where the initial conditions, $\epsilon^0(\sigma^0)$ and $\epsilon_e^0(\sigma^0)$, are determined by integration of Eqs. (16), (17) and (29) from $\sigma = 0$ to $\sigma = \sigma^0$.

Given a stress σ^0 , Eqs. (2), (5), (30), (32) and (33) are characterized by 4 adjustable parameters:

1. the average potential energy for separation of active strands Ω ,
2. the standard deviation of potential energies of active MRs Σ ,
3. the concentration of active meso-domains κ_a ,
4. the attempt rate for detachment of strands from temporary junctions Γ_a .

It follows from Eqs. (2), (5), (30) and (32) that the quantities Ω and Γ_a are mutually dependent: an increase in Ω results in an increase in Γ_a . To reduce the number of material constants to be found by matching observations in creep tests, we set $\Gamma_a = 1$ s. Our purpose now is to find adjustable parameters E , a , b , κ_a , Ω and Σ by fitting experimental data depicted in Figures 1 to 3.

6 Fitting of observations

We begin with the approximation of the stress–strain curves presented in Figure 1. Under uniaxial tension with the cross-head speed 5 mm/min, the strain $\epsilon_{\max} = 0.06$ is reached within 69 s. According to Figures 2 and 3, changes in strain induced by rearrangement of active strands during this period are insignificant at stresses up to 20 MPa, whereas the duration of stretching at higher stresses does not exceeds 30 s, which causes rather small growth of strains. Based on these observations, we treat the deformation process as rapid and apply Eqs. (16), (17) and (29) to fit experimental data.

For any temperature of annealing, T , the stress–strain curve is matched independently. To find the constants E , a and b , we fix the intervals $[0, a_{\max}]$ and $[0, b_{\max}]$, where the “best-fit” parameters a and b are assumed to be located, and divide these intervals into J subintervals by the points $a_i = i\Delta a$ and $b_j = j\Delta b$ ($i, j = 1, \dots, J$) with $\Delta a = a_{\max}/J$ and $\Delta b = b_{\max}/J$. For any pair, $\{a_i, b_j\}$, we integrate the governing equations numerically (with the step $\Delta\epsilon = 5.0 \cdot 10^{-5}$) by the Runge–Kutta method. The elastic modulus

$E = E(i, j)$ is found by the least-squares algorithm from the condition of minimum of the function

$$K(i, j) = \sum_{\epsilon_m} [\sigma_{\text{exp}}(\epsilon_m) - \sigma_{\text{num}}(\epsilon_m)]^2,$$

where the sum is calculated over all experimental points, ϵ_m , depicted in Figure 1, σ_{exp} is the longitudinal stress measured in a tensile test, and σ_{num} is given by Eq. (29). The “best-fit” parameters a and b minimize K on the set $\{a_i, b_j \mid (i, j = 1, \dots, J)\}$. After determining their values, a_i and b_j , this procedure is repeated twice for the new intervals $[a_{i-1}, a_{i+1}]$ and $[b_{j-1}, b_{j+1}]$ to ensure an acceptable accuracy of fitting.

The “best-fit” parameters E , $\epsilon_* = a^{-1}$ and b are plotted in Figures 4 to 6 as functions of the annealing temperature T . The experimental data are approximated by the linear functions

$$E = E_0 + E_1 T, \quad \epsilon_* = \epsilon_{*0} + \epsilon_{*1} T, \quad b = b_0 + b_1 T, \quad (34)$$

where the coefficients E_m , ϵ_{*m} and b_m ($m = 0, 1$) are determined by the least-squares technique.

We proceed with fitting the creep curves for non-annealed specimens depicted in Figure 2. For any stress, σ^0 , the quantities ϵ^0 and ϵ_{ep}^0 are found by integration of Eqs. (16), (17) and (29) with the material constants found in the approximation of the stress–strain curve plotted in Figure 1. To determine $\Omega(\sigma^0)$, $\Sigma(\sigma^0)$ and $\kappa(\sigma^0)$, the following algorithm is employed. We fix the intervals $[0, \Omega_{\text{max}}]$, $[0, \Sigma_{\text{max}}]$ and $[0, \kappa_{\text{max}}]$, where the “best-fit” parameters Ω , Σ and κ are assumed to be located, and divide these intervals into J subintervals by the points $\Omega_i = i\Delta\Omega$, $\Sigma_j = j\Delta\Sigma$ and $\kappa_k = k\Delta\kappa$ ($i, j, k = 1, \dots, J$) with $\Delta\Omega = \Omega_{\text{max}}/J$, $\Delta\Sigma = \Sigma_{\text{max}}/J$ and $\Delta\kappa = \kappa_{\text{max}}/J$. For any pair, $\{\Omega_i, \Sigma_j\}$, the constant $p^0 = p^0(i, j)$ is found from Eq. (6), where the integral is evaluated by Simpson’s method with 200 points and the step $\Delta\omega = 0.15$. For any triple, $\{\Omega_i, \Sigma_j, \kappa_k\}$, Eqs. (2), (5), (30), (32) and (33) are integrated numerically (with the time step $\Delta t = 0.1$) by the Runge–Kutta method. The “best-fit” parameters Ω , Σ and κ minimize the function

$$K(i, j, k) = \sum_{t_m} [\epsilon_{\text{exp}}(t_m) - \epsilon_{\text{num}}(t_m)]^2,$$

where the sum is calculated over all experimental points, t_m , presented in Figure 2, ϵ_{exp} is the strain measured in the creep test, and ϵ_{num} is given by Eq. (33). After determining the “best-fit” values, Ω_i , Σ_j and κ_k , this procedure is repeated for the new intervals $[\Omega_{i-1}, \Omega_{i+1}]$, $[\Sigma_{j-1}, \Sigma_{j+1}]$ and $[\kappa_{k-1}, \kappa_{k+1}]$, to provide an acceptable accuracy of fitting.

The adjustable parameters Ω , Σ and κ are plotted versus the engineering stress, σ , in Figures 7 to 9. The experimental data are approximated by the linear functions

$$\Omega = \Omega_0 + \Omega_1 \sigma, \quad \Sigma = \Sigma_0 + \Sigma_1 \sigma, \quad \kappa = \kappa_0 + \kappa_1 \sigma, \quad (35)$$

where the coefficients Ω_m , Σ_m and κ_m ($m = 0, 1$) are found by the least-squares technique.

Finally, we approximate the experimental data in creep tests on specimens annealed for 24 h at $T = 140$ °C presented in Figure 3. To determine adjustable parameters in the constitutive equations, the same procedure of fitting is used as for the observations depicted in Figure 2. The “best-fit” quantities Ω , Σ and κ are plotted versus the stress σ in Figures 7 to 9 together with their approximations by Eqs. (35).

7 Discussion

Figure 1 demonstrates fair agreement between the observations in tensile tests with a constant strain rate and the results of numerical simulation.

Figure 4 shows that the elastic modulus E monotonically increases with annealing temperature T . In the region of temperatures from room temperature to 130 °C, this increase is rather small, but the rate of growth in $E(T)$ substantially increases in the interval of temperatures between 130 and 150 °C. This conclusion is in agreement with observations in calorimetric tests by other researchers, which reveal that the melting temperature, T_m , monotonically grows with crystallization temperature, T , and the slope of the curve $T_m(T)$ noticeably increases at the temperature $T = 130$ °C. Results of three DSC (differential scanning calorimetry) studies on iPP are presented in Figure 10. In this figure, the dependence of the melting peak, T_m , on the crystallization temperature, T , is approximated by the linear function

$$T_m = c_0 + c_1 T. \quad (36)$$

The coefficients c_m ($m = 0, 1$) in Eq. (36) are found by using the least-squares algorithm.

According to the Gibbs–Thomson theory (see, e.g., [5, 7]), an increase in the equilibrium melting temperature, T_m , is tantamount to an increase in the average lamellar thickness. Comparing Figures 4 and 10, we draw a conclusion that the growth of the elastic modulus of iPP with annealing temperature may be attributed to lamellar thickening.

Figures 5 and 6 reveal that the plastic strain, ϵ_* , and the rate of developed plastic flow, b , decrease in the interval from 110 to 130 °C and increase at higher temperatures. Two possible explanations may be provided for the decrease in ϵ_* :

1. According to Labour et al. [24], annealing of isotactic polypropylene in the range of temperatures between 110 and 130 °C results in an increase in the concentration of ductile β spherulites that enhance plastic flow. This phenomenon is explained by the fact that “in the hexagonal phase, the chains are loosely packed, which suggests that chains are mobile” [34]. At annealing above 130 °C, development of β spherulites is thermodynamically unfavorable (Al-Raheil et al. [2] reported that “no β spherulites were found above the crystallization temperature 132 °C”), which implies an increase in ϵ_* and a corresponding decrease in elastoplastic deformations.
2. Men and Strobl [33] recently suggested that development of subsidiary lamellae at annealing is a two-step process consisting of formation of lamellar blocks at the initial stage and their aggregation into a “blocky substructure” at the final stage. According to this scenario, enhancement of plastic flow at low-temperature annealing is attributed to sliding of isolated lamellar blocks formed at secondary crystallization (the duration of thermal pre-treatment at temperatures in the range of 110 to 130 °C is assumed to be insufficient for the development of a blocky structure), whereas its decay at annealing above 130 °C is ascribed to aggregation of these blocks into stacks of relatively rigid lamellae.

Both explanations are rather far from being exhausted. The first is based on the assumption that β spherulites grow at low-temperature annealing, which was questioned in

several works, see, e.g., [5] and the references therein. The other explanation presumes a new mechanism for development of subsidiary lamellae, which has not yet been confirmed experimentally. It is worth also noting that these models do not establish links between changes in the plastic strain, ϵ_* , and appropriate alternations in the rate of plastic flow, b .

A decrease in the rate of steady plastic flow, b , with temperature of annealing below 130 °C is attributed to lamellar thickening, which results in slowing down of the developed plastic flow (which is associated with lamellar fragmentation and motion of isolated lamellar blocks). An increase in b at higher temperatures is explained by the fact that at high-temperature annealing two processes occur simultaneously: (i) thickening of dominant lamellae and growth of subsidiary lamellae and (ii) annihilation of transverse lamellae. Gu et al. [7] reported that annealing of iPP in the high-temperature region leads to “the complete absence of the cross-hatching.” This implies a substantial reduction in the rigidity of spherulites, and, as a consequence, an enhancement of the developed plastic flow.

To assess the level of elastoplastic strains at stretching of iPP specimens annealed at different temperatures, we integrate Eqs. (16) and (17) with adjustable parameters determined by matching experimental data in tensile tests. The results of numerical simulation are presented in Figure 11. This figure reveals that the elastoplastic strain, ϵ_p , is practically independent of annealing temperature (although the stress–strain diagrams depicted in Figure 1 are strongly affected by thermal pre-treatment).

Figure 7 demonstrates that the average activation energy for separation of strands from temporary nodes, Ω , decreases with stress, σ , for non-annealed samples and increases for specimens annealed at 140 °C. This qualitative difference in the dependence $\Omega(\sigma)$ for annealed and non-annealed iPP may be associated with transformation of smectic mesophase into lamellar blocks during thermal treatment. In a stress-free non-annealed specimen, the concentration of flocks of smectic mesophase (“arrays of chains with a better order in longitudinal than in transverse chain direction” [35]) is rather large. These ordered arrays of macromolecules slow down rearrangement of strands in active MRs, which implies that at small stresses, the average activation energy of samples not subjected to thermal treatment is rather large. According to the Men–Strobl model [33], annealing of specimens results in transformation of smectic mesophase into lamellar blocks and subsidiary lamellae. This transformation of “clusters of slow junctions” in amorphous regions into the crystalline phase enhances the rearrangement process, which implies that at small stresses, Ω for non-annealed specimens substantially exceeds that for annealed samples.

With an increase in stress, clusters of smectic mesophase in amorphous regions are disintegrated, and these “ordered” chains are transformed into ordinary ones. This process enhances detachment of strands from temporary junctions, which is reflected by a decrease in the average potential energy of active meso-domains.

On the contrary, the growth of longitudinal stress results in fragmentation of “weak” lamellar blocks formed from smectic mesophase at annealing. Pieces of broken lamellar blocks distributed in amorphous regions serve as extra physical cross-links with high activation energy for separation of strands. As a result, stretching of annealed specimens increases the potential energy for detachment of chains and slows down the rearrangement

process.

This scenario is confirmed by experimental data for the standard deviation of potential energies of active meso-domains depicted in Figure 8. This figure reveals that Σ decreases with stress for non-annealed specimens (which is attributed to destruction of clusters of smectic mesophase in amorphous regions) and increases with stress for annealed samples (which is ascribed to the growth of concentration of extra physical cross-links induced by breakage of “weak” lamellar blocks).

For the quasi-Gaussian distribution function (5), Ω and Σ may be treated as an apparent average potential energy for detachment of active strands, and an apparent standard deviation of potential energies for separation of strands from the network. The average activation energy, Ω_0 , and the standard deviation of activation energies, Σ_0 , are given by

$$\Omega_0 = \int_0^\infty \omega p(\sigma^0, \omega) d\omega, \quad \Sigma_0 = \left[\int_0^\infty (\omega - \Omega_0)^2 p(\sigma^0, \omega) d\omega \right]^{\frac{1}{2}}.$$

We determine the dimensionless quantities Ω_0 and Σ_0 according to these formulas and calculate the ratio

$$\xi = \frac{\Sigma_0}{\Omega_0}$$

that characterizes the width of the quasi-Gaussian distribution. The parameter ξ is plotted versus stress, σ , in Figure 11. The experimental data are approximated by the linear function

$$\xi = \xi_0 + \xi_1 T, \quad (37)$$

where the coefficients ξ_m ($m = 0, 1$) are found by the least-squares technique. Figure 11 demonstrates that the width of the distribution of active MRs, Eq. (5), is practically not affected by thermal treatment, and it weakly increases with longitudinal stress. The rate of increase in ξ with stress appears to be independent of annealing temperature.

Figure 9 reveals qualitatively different effects of the longitudinal stress on the concentration of active meso-regions, κ , for non-annealed specimens and for specimens subjected to thermal pre-treatment. For non-annealed specimens, κ remains constant up to $\sigma_* \approx 18$ MPa and linearly decreases with stress at higher longitudinal stresses. For specimens, annealed at 140 °C, κ slightly increases with stress in the entire interval of deformations under consideration.

At relatively small stresses, $\sigma < \sigma_*$, the fraction of active meso-domains in non-annealed specimens noticeably exceeds that for annealed samples. This conclusion is explained by the fact that annealing of iPP results in secondary crystallization of a part of the amorphous phase, which implies that the content of active MRs is reduced. An increase in κ with stress for annealed specimens is also quite natural, because it is associated with mechanically-induced fragmentation of weak lamellae and release of the amorphous phase, whose rearrangement was prevented by surrounding lamellae in a stress-free specimen.

To explain a pronounced decrease in κ for non-annealed specimens at stresses exceeding σ_* , we should recall that the fitting procedure presumed the quantities Ω , Σ and κ in Eqs. (5) and (30) to be uniquely determined by stress, σ , and to be independent of elastoplastic strain, ϵ_p . To assess, whether this hypothesis is adequate, we integrate

numerically Eqs. (2), (5), (30), (32) and (33) with the adjustable parameters found by matching observations and calculate the elastoplastic strain, ϵ_p , as a function of time, t . The results of numerical simulation are depicted in Figures 13 and 14.

Figure 14 shows that for all stresses (except for the highest stress, $\sigma = 30$ MPa), the elastoplastic strain, ϵ_p , slightly increases with time in a fashion typical of primary creep. Curve 5 in this figure demonstrates a transition from the primary creep to the secondary creep (a linear increase in ϵ_p with time) at the final stage of the creep test.

In contrast with results presented in Figure 14, Figure 13 reveals that ϵ_p increases with time following the primary-creep mode only at relatively small stresses ($\sigma < \sigma_*$). At higher stresses, the primary creep is transformed into the secondary creep (curves 4 and 5), and, finally, into the ternary creep (curve 6).

Based on this observation, one can conclude that below the critical stress, σ_* , the concentration of active MRs, κ , is independent of the elastoplastic strain, ϵ_p . This implies that in the interval of stresses $[0, \sigma_*]$, κ remains constant (in agreement with the experimental data plotted in Figure 9). The independence of κ of longitudinal stress, σ , in this interval may be ascribed to the fact that at relatively small deformations smectic mesophase is mainly rearranged, while dominant lamellae (that restrict mobility of amorphous meso-domains) remain undisturbed.

Above the critical stress, σ_* , i.e., in the region of secondary and ternary creep flows, the parameter κ becomes a function of two arguments: the longitudinal stress, σ , and the elastoplastic strain, ϵ_p . This implies that the data for κ depicted in Figure 9 at $\sigma > \sigma_*$ should be treated as “average” (over the creep curves) quantities. This means that the noticeable decrease in κ (curve 1b in Figure 9) should be attributed to the influence of secondary and ternary creep flows on rearrangement of strands in active MRs.

The following scenario may be proposed for a decrease in κ observed in creep tests at relatively large stresses. A pronounced growth of elastoplastic strain ϵ_p (curves 4 to 6 in Figure 13) is associated with fragmentation of dominant lamellae and plastic flow of lamellar blocks. In contrast with annealed specimens, where primary lamellae are broken into small pieces that serve as extra physical cross-links in active MRs (curves 2 in Figures 7 and 8), dominant lamellae in specimens not subjected to thermal treatment are assumed to be disintegrated into relatively large blocks whose average length is comparable with the characteristic size of active MRs. Plastic flow of these blocks results in confining of some amorphous regions, where rearrangement of strands becomes prevented by surrounding immobile lamellae and moving lamellar blocks. This confinement of active MRs is temporary: when a lamellar block moves away from a “trapped” meso-region, it is released, and the rearrangement process proceeds. However, the higher the plastic strain, ϵ_p , is, the large is the number of “moving lamellar blocks,” and, as a consequence, the smaller is the concentration of active MRs.

According to this picture, an increase in the content of active meso-domains with stress for annealed samples is attributed to breakage of lamellae into small blocks, whereas a decrease in κ with stress for non-annealed specimens is ascribed to fragmentation of lamellae into large blocks, whose size is comparable with that of active MRs. This difference in the processes of lamellar disintegration for annealed and non-annealed samples is in agreement with the micro-mechanisms of lamellar growth at secondary crystallization recently proposed by Hikosaka et al. [34]. According to it, lamellar thickening is accompanying by

transformation of folded chain crystals in the lamellar cores into extended chain crystals. Packing of extended chains in the central part of a growing lamella becomes substantially looser compared to the initial one, which implies that dominant lamellae after thickening at secondary crystallization are fragmented into noticeably smaller pieces than the same lamellae before annealing.

8 Concluding remarks

A model has been developed for the elastoplastic and viscoelastic responses of semicrystalline polymers at isothermal loading. A complicated micro-structure of a semi-crystalline polymer is replaced by an equivalent transient network of macromolecules bridged by junctions (physical cross-links, entanglements and crystalline lamellae). The network is thought of as an ensemble of meso-regions with various potential energies for separation of strands from temporary nodes.

The viscoelastic response of a semicrystalline polymer is attributed to (i) detachment of active strands from temporary nodes in active meso-domains and (ii) merging of dangling strands with the network. Rearrangement of strands is treated as a thermally activated process, whose rate is determined by the Eyring equation (2).

The elastoplastic behavior is ascribed to slippage of junctions with respect to their positions in the bulk material. Kinetic equation (16) is proposed for the rate of sliding, where the plastic flow is governed by the elastic strain (not stress, as in conventional theories of plasticity).

Stress-strain relation (28) has been developed for isothermal uniaxial deformation by using the laws of thermodynamics. Adjustable parameters in the constitutive equations are found by fitting experimental data in tensile tests with a constant strain rate and in creep tests.

A series of tensile tests has been performed on isotactic polypropylene at room temperature. The mechanical experiments are carried out on injection-molded specimens not subjected to thermal treatment and on samples annealed for 24 h at the temperatures 110, 120, 130, 140 and 150 °C.

Two series of creep tests have been performed on non-annealed specimens and on specimens annealed at 140 °C in the interval of stresses from 10 to 30 MPa. Fair agreement is demonstrated between the experimental data and the results of numerical simulation.

The following conclusions are drawn:

1. The flow rule (15), (16) and (29) with 3 adjustable parameters correctly describes observations in “rapid” tensile tests, when the effect of material viscosity is negligible. The elastic modulus, E , increases with annealing time (which is attributed to lamellar thickening), whereas the plastic strain, ϵ_* , and the rate of developed plastic flow, b , demonstrate a more sophisticated behavior: they linearly decrease with annealing temperature, T , below $T_c = 130$ °C and increase above T_c . The temperature T_c roughly coincides with the temperature, at which the rate of lamellar thickening noticeably increases.

2. The governing equations (2), (5), (30), (32) and (33) with 3 material constants adequately describe experimental data in creep tests under the assumption that the quantities Ω , Σ and κ are stress-dependent. The average activation energy for separation of chains from temporary nodes, Ω , increases with stress for annealed specimens and decreases for samples not subjected to thermal treatment. This difference is attributed to different mechanisms of lamellar fragmentation into blocks. The width of the quasi-Gaussian distribution (5) is weakly affected by longitudinal stress and annealing temperature.
3. The concentration of active meso-domains, κ , grows with stress for annealed specimens. This parameter is stress-independent for non-annealed samples below the threshold stress, σ_* , and decreases with stress at $\sigma > \sigma_*$. The latter observation is ascribed to transition from the primary creep of non-annealed specimens to the secondary and tertiary creep flows, when rearrangement of strands in active MRs becomes strongly affected by elastoplastic strains.

References

- [1] G. Kalay, M.J. Bevis, *J. Polym. Sci. B: Polym. Phys.* 35 (1997) 241, 265.
- [2] I.A. Al-Raheil, A.M. Qudah, M. Al-Share, *J. Appl. Polym. Sci.* 67 (1998) 1259, 1267.
- [3] J. Xu, S. Srinivas, H. Marand, P. Agarwal, *Macromolecules* 31 (1998) 8230.
- [4] R.G. Alamo, G.M. Brown, L. Mandelkern, A. Lehtinen, R. Paukkerri, *Polymer* 40 (1999) 3933.
- [5] M. Iijima, G. Strobl, *Macromolecules* 33 (2000) 5204.
- [6] P. Maiti, M. Hikosaka, K. Yamada, A. Toda, F. Gu, *Macromolecules* 33 (2000) 9069.
- [7] F. Gu, M. Hikosaka, A. Toda, S.K. Ghosh, S. Yamazaki, M. Arakaki, K. Yamada, *Polymer* 43 (2002) 1473.
- [8] I.M. Ward, J.M. Wolfe, *J. Mech. Phys. Solids* 14 (1966) 131.
- [9] J. Smart, J.G. Williams, *J. Mech. Phys. Solids* 20 (1972) 313.
- [10] F.-J. Wortmann, K.V. Schulz, *Polymer* 35 (1994) 2108.
- [11] F.-J. Wortmann, K.V. Schulz, *Polymer* 36 (1995) 2363.
- [12] T. Ariyama, *J. Mater. Sci.* 31 (1996) 4127.
- [13] T. Ariyama, Y. Mori, K. Kaneko, *Polym. Eng. Sci.* 37 (1997) 81.
- [14] N.K. Dutta, G.H. Edward, *J. Appl. Polym. Sci.* 66 (1997) 1101.
- [15] B.E. Read, P.E. Tomlins, *Polymer* 38 (1997) 4617.
- [16] P.E. Tomlins, B.E. Read, *Polymer* 39 (1998) 355.
- [17] J. Sweeney, T.L.D. Collins, P.D. Coates, R.A. Duckett, *J. Appl. Polym. Sci.* 72 (1999) 563.
- [18] M. Aboulfaraj, C. G'Sell, B. Ulrich, A. Dahoun, *Polymer* 36 (1995) 731.
- [19] G. Coulon, G. Castelein, C. G'Sell, *Polymer* 40 (1998) 95.
- [20] R. Seguela, E. Staniek, B. Escaig, B. Fillon, *J. Appl. Polym. Sci.* 71 (1999) 1873.
- [21] E. Staniek, R. Seguela, B. Escaig, P. Francois, *J. Appl. Polym. Sci.* 72 (1999) 1241.
- [22] K.-H. Nitta, M. Takayanagi, *J. Polym. Sci. B: Polym. Phys.* 37 (1999) 357.
- [23] K.-H. Nitta, M. Takayanagi, *J. Polym. Sci. B: Polym. Phys.* 38 (2000) 1037.
- [24] T. Labour, C. Gauthier, R. Seguela, G. Vigier, Y. Bomal, G. Orange, *Polymer* 42 (2001) 7127.

- [25] R. Verma, H. Marand, B. Hsiao, *Macromolecules* 29 (1996) 7767.
- [26] X.C. Zhang, M.F. Butler, R.E. Cameron, *Polym. Int.* 48 (1999) 1173.
- [27] R.W. Meyer, L.A. Pruitt, *Polymer* 42 (2001) 5293.
- [28] J. Sweeney, I.M. Ward, *J. Mech. Phys. Solids* 44 (1996) 1033.
- [29] E. Andreassen, *Polymer* 40 (1999) 3909.
- [30] F. Tanaka, S.F. Edwards, *Macromolecules* 25 (1992) 1516.
- [31] E.M. Arruda, M.C. Boyce, R. Jayachandran, *Mech. Mater.* 19 (1995) 193.
- [32] A.S. Krausz, H. Eyring, *Deformation Kinetics*. Wiley, New York (1975).
- [33] Y. Men, G. Strobl, *Polymer*, 43 (2002) 2761.
- [34] M. Hikosaka, K. Amano, S. Rastogi, A. Keller, *Macromolecules* 30 (1997) 2067.
- [35] R. Androsch, B. Wunderlich, *Macromolecules* 34 (2001) 5950.

List of figures

Figure 1: The stress σ MPa versus strain ϵ in tensile tests. Circles: experimental data. Curve 1: a non-annealed specimen; curves 2 to 6: specimens annealed at a temperature T °C. Curve 2: $T = 110$; curve 3: $T = 120$; curve 4: $T = 130$; curve 5: $T = 140$; curve 6: $T = 150$. Solid lines: results of numerical simulation

Figure 2: The strain ϵ versus time t s in a tensile creep test with a stress σ MPa. Circles: experimental data for non-annealed specimens. Solid lines: results of numerical simulation. Curve 1: $\sigma = 10.0$; curve 2: $\sigma = 15.0$; curve 3: $\sigma = 17.5$; curve 4: $\sigma = 20.0$; curve 5: $\sigma = 22.5$; curve 6: $\sigma = 25.0$

Figure 3: The strain ϵ versus time t s in a tensile creep test with a stress σ MPa. Circles: experimental data for specimens annealed at $T = 140$ °C. Solid lines: results of numerical simulation. Curve 1: $\sigma = 10.0$; curve 2: $\sigma = 15.0$; curve 3: $\sigma = 20.0$; curve 4: $\sigma = 25.0$; curve 5: $\sigma = 30.0$

Figure 4: The elastic modulus E GPa versus annealing temperature T °C. Circles: treatment of observations. Solid lines: approximation of the experimental data by Eq. (34). Curve 1: $E_0 = 2.0242$, $E_1 = 0.0010$; curve 2: $E_0 = 0.4946$, $E_1 = 0.0129$

Figure 5: The plastic strain ϵ_* versus annealing temperature T °C. Circles: treatment of observations. Solid lines: approximation of the experimental data by Eq. (34). Curve 1: $\epsilon_{*0} = 3.53 \cdot 10^{-2}$, $\epsilon_{*1} = -1.08 \cdot 10^{-4}$; curve 2: $\epsilon_{*0} = 8.68 \cdot 10^{-3}$, $\epsilon_{*1} = 1.04 \cdot 10^{-4}$

Figure 6: The rate of developed plastic flow b versus annealing temperature T °C. Circles: treatment of observations. Solid lines: approximation of the experimental data by Eq. (34). Curve 1: $b_0 = 0.9614$, $b_1 = -0.0018$; curve 2: $b_0 = 0.4657$, $b_1 = 0.0021$

Figure 7: The average potential energy for detachment of strands Ω versus stress σ MPa. Symbols: treatment of observations. Unfilled circles: non-annealed specimens; filled circles: specimens annealed at $T = 140$ °C. Solid lines: approximation of the experimental data by Eq. (35). Curve 1: $\Omega_0 = 8.5079$, $\Omega_1 = -0.1756$; curve 2: $\Omega_0 = 4.3232$, $\Omega_1 = 0.0950$

Figure 8: The standard deviation of potential energies for separation of strands Σ versus stress σ MPa. Symbols: treatment of observations. Unfilled circles: non-annealed specimens; filled circles: specimens annealed at $T = 140$ °C. Solid lines: approximation of the experimental data by Eq. (35). Curve 1: $\Sigma_0 = 4.4272$, $\Sigma_1 = -0.0811$; curve 2: $\Sigma_0 = 0.8672$, $\Sigma_1 = 0.1347$

Figure 9: The concentration of active MRs κ versus stress σ MPa. Symbols: treatment of observations. Unfilled circles: non-annealed specimens; filled circles: specimens annealed at $T = 140$ °C. Solid lines: approximation of the experimental data by Eq. (35). Curve 1a: $\kappa_0 = 0.48$, $\kappa_1 = 0.0$; curve 1b: $\kappa_0 = 1.1052$, $\kappa_1 = -0.0367$; curve 2: $\kappa_0 = 0.2371$, $\kappa_1 = 0.0057$

Figure 10: The melting peak T_m °C versus crystallization temperature T °C. Symbols: treatment of observations for isotactic polypropylene. Unfilled circles: iPP crystallized for 22 h at temperature T and cooled to room temperature [2]; filled circles: iPP crystallized for an unspecified time at temperature T [5]; asterisks: iPP crystallized for 100 min at temperature T [3]. Solid lines: approximation of the experimental data by Eq. (36).

Vertical lines indicate transition temperatures

Figure 11: The elastoplastic strain ϵ_p versus strain ϵ in tensile tests on specimens annealed at various temperatures T . Solid lines: results of numerical simulation

Figure 12: The ratio ξ versus stress σ MPa. Symbols: treatment of observations. Unfilled circles: non-annealed specimens; filled circles: specimens annealed at $T = 140$ °C. Solid lines: approximation of the experimental data by Eq. (37). Curve 1: $\xi_0 = 0.4643$, $\xi_1 = 0.0014$; curve 2: $\xi_0 = 0.4369$, $\xi_1 = 0.0011$

Figure 13: The elastoplastic strain ϵ_p versus time t s in a tensile creep test with a stress σ MPa. Solid lines: results of numerical simulation for non-annealed specimens. Curve 1: $\sigma = 10.0$; curve 2: $\sigma = 15.0$; curve 3: $\sigma = 17.5$; curve 4: $\sigma = 20.0$; curve 5: $\sigma = 22.5$; curve 6: $\sigma = 25.0$

Figure 14: The elastoplastic strain ϵ_p versus time t s in a tensile creep test with a stress σ MPa. Solid lines: results of numerical simulation for specimens annealed at 140 °C. Curve 1: $\sigma = 10.0$; curve 2: $\sigma = 15.0$; curve 3: $\sigma = 20.0$; curve 4: $\sigma = 25.0$; curve 5: $\sigma = 30.0$

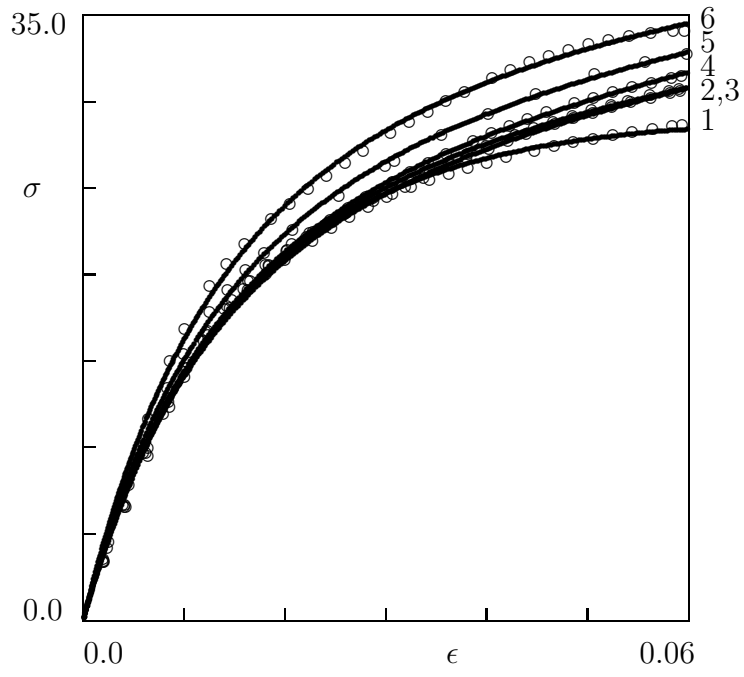


Figure 1:

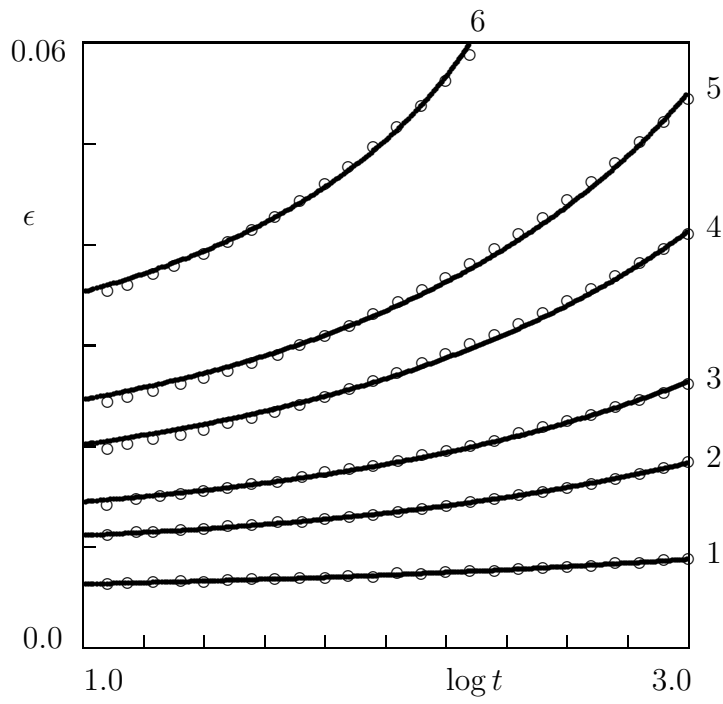


Figure 2:

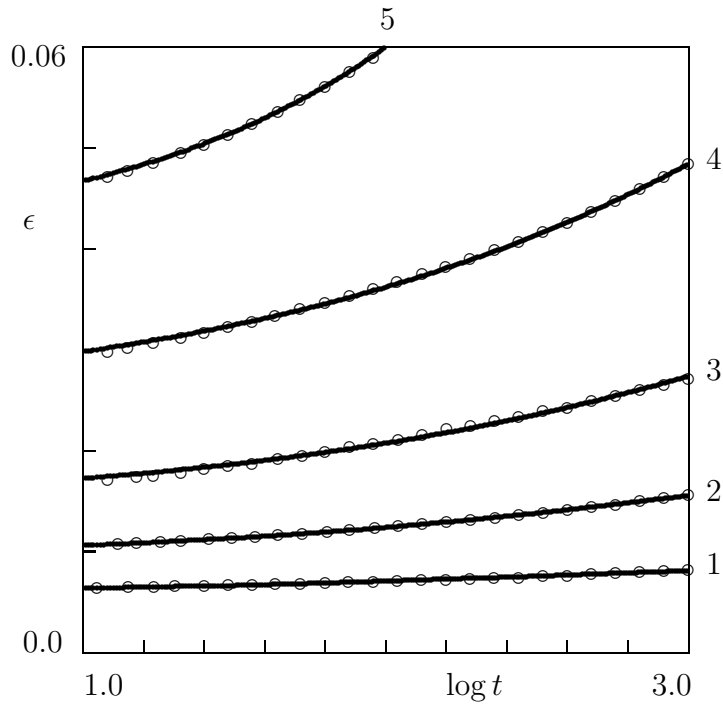


Figure 3:

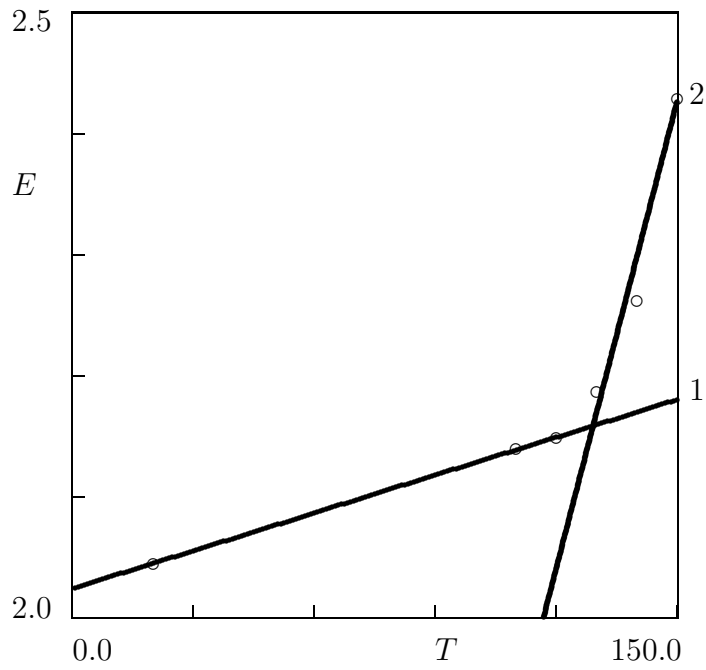


Figure 4:

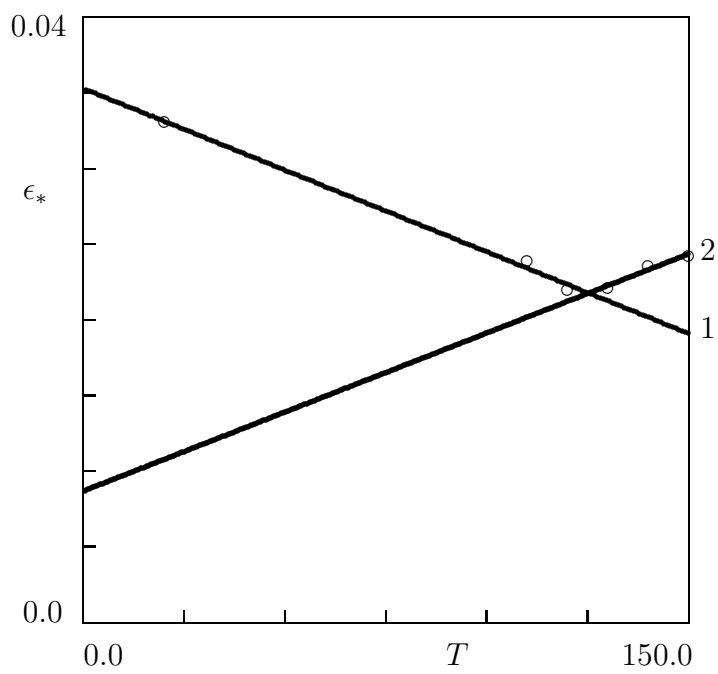


Figure 5:

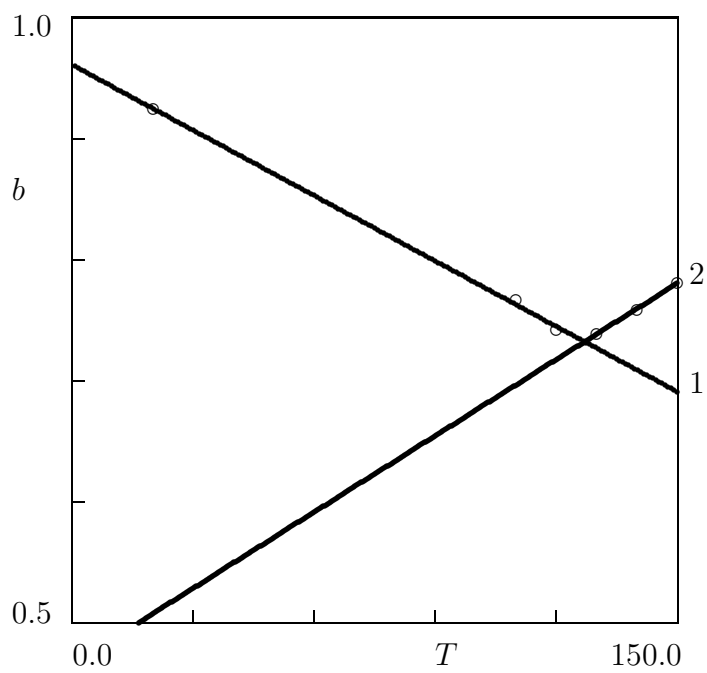


Figure 6:

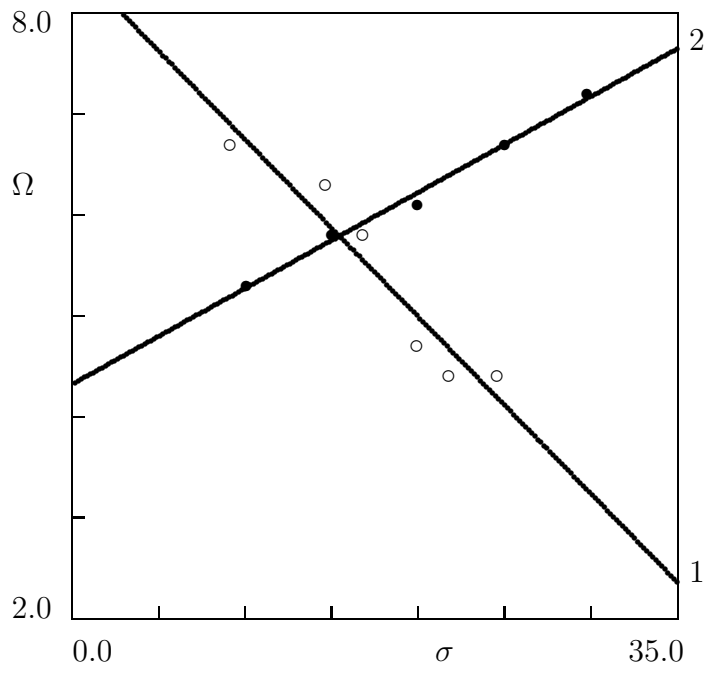


Figure 7:

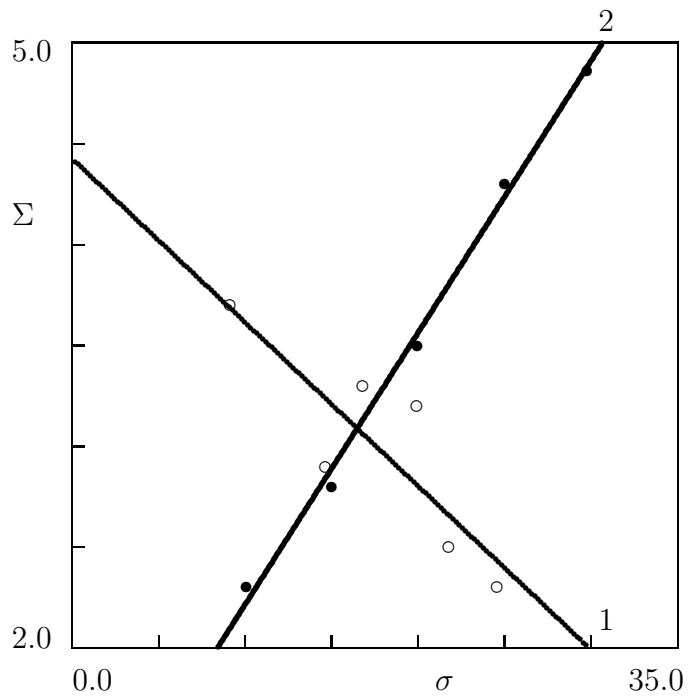


Figure 8:

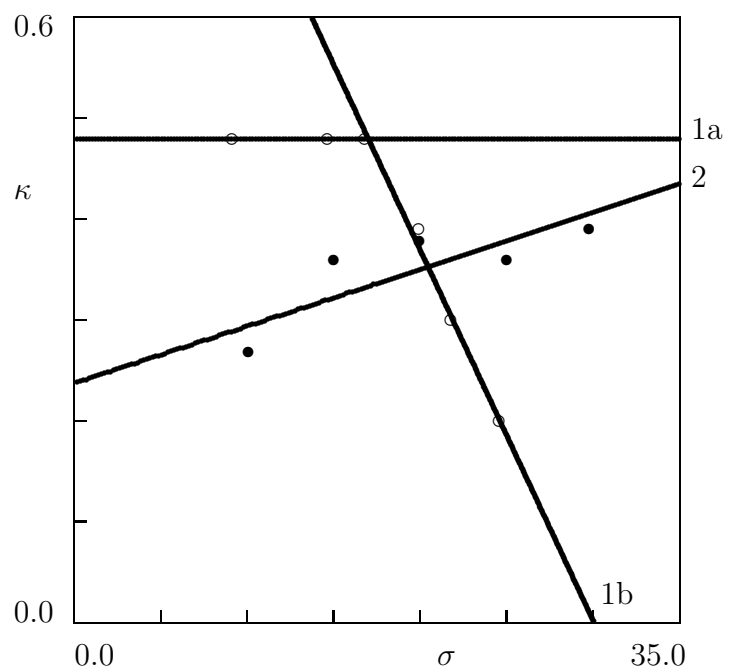


Figure 9:

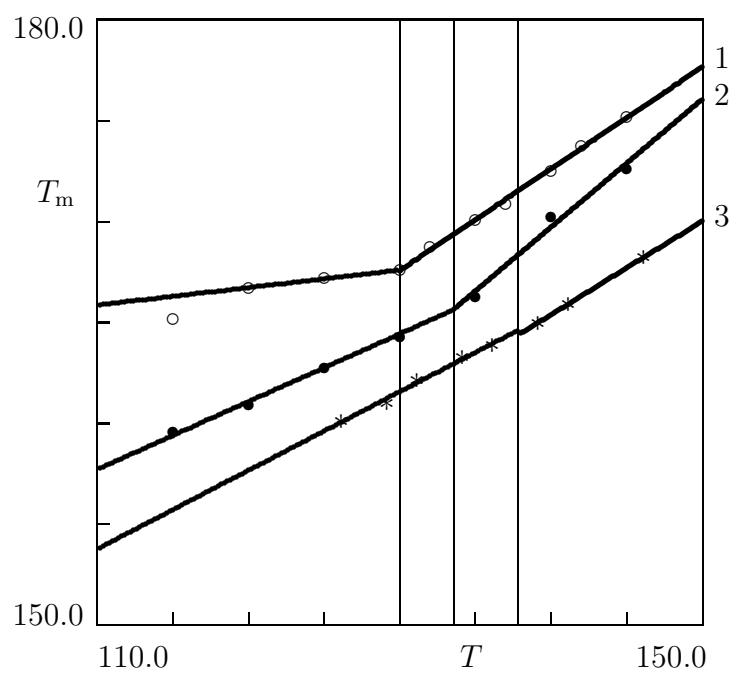


Figure 10:

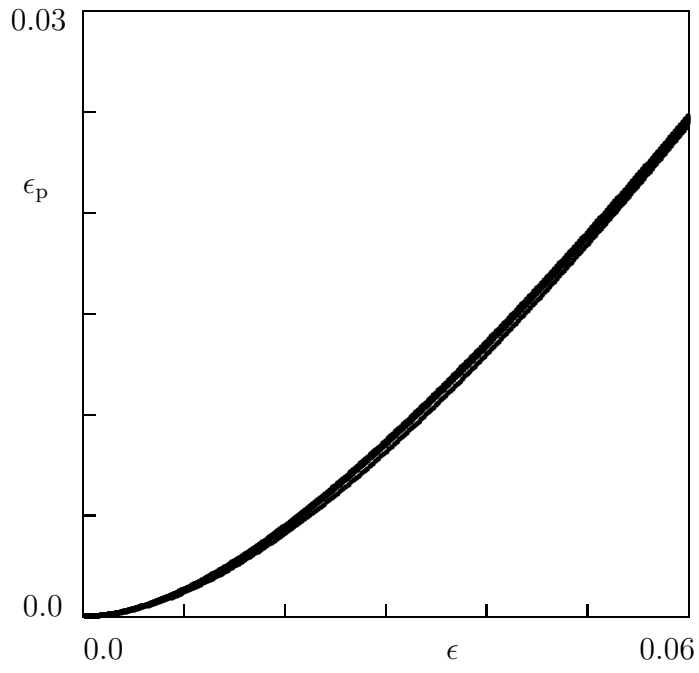


Figure 11:

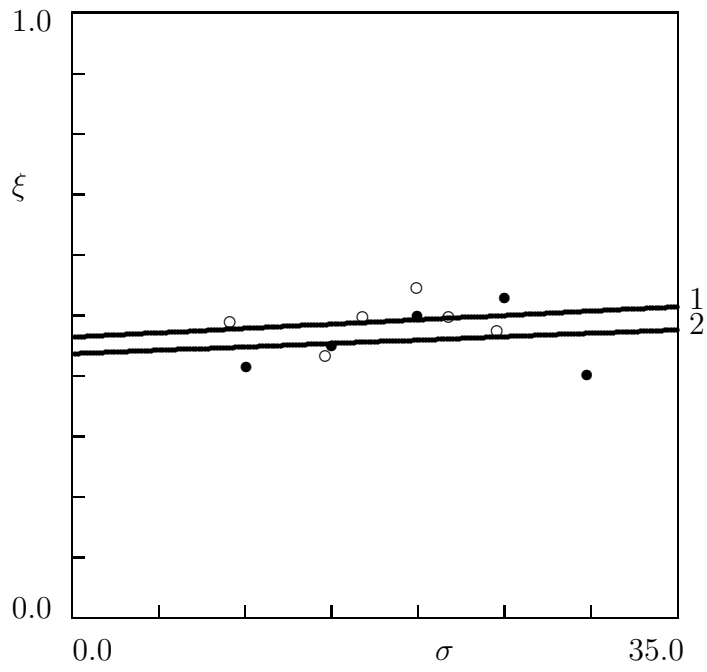


Figure 12:

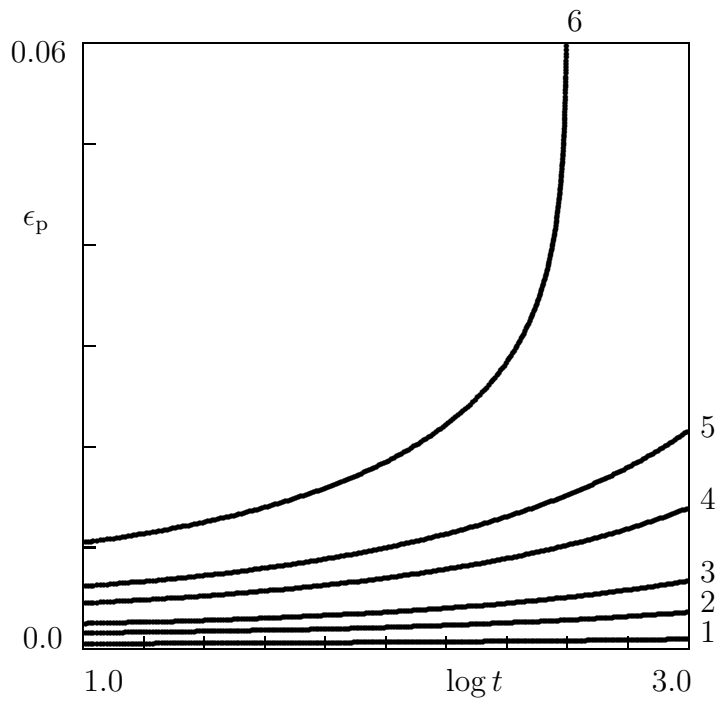


Figure 13:

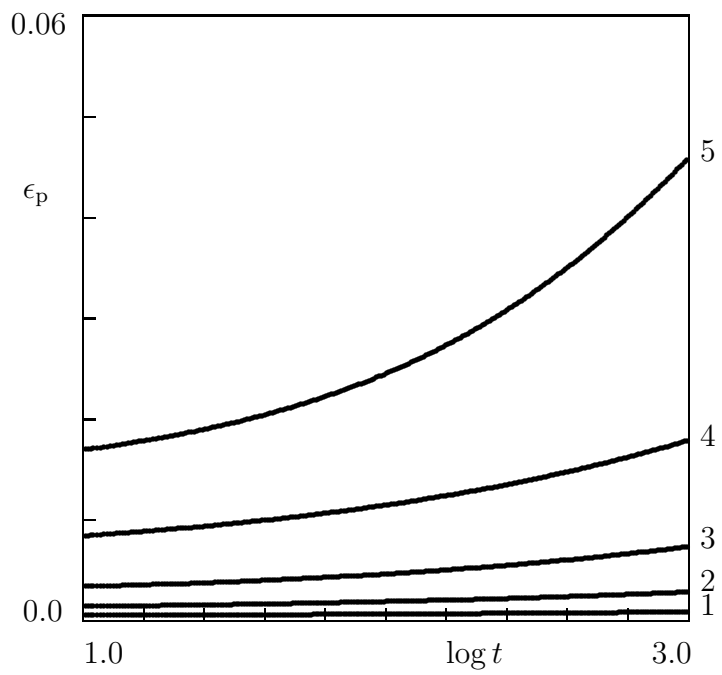


Figure 14: